

Control of the 2009 L'Aquila earthquake, central Italy, by a high-velocity structure: A receiver function study

I. Bianchi,¹ C. Chiarabba,¹ and N. Piana Agostinetti¹

Received 4 November 2009; revised 10 September 2010; accepted 22 September 2010; published 29 December 2010.

[1] Receiver functions (RFs) analyzed at two permanent broadband seismic stations operating in the epicentral area of the M_w 6.3, 2009 L'Aquila earthquake (central Italy) yield insight on crustal structure along the fault rupture. The harmonic decomposition of RFs highlights a subsurface structure in which both isotropic and anisotropic features are present. We model the waveforms using recently developed Monte Carlo methods. The retrieved models display a common depth structure, between 10 and 40 km depth, consistent with the under-thrusting of the Adria lithosphere underneath the Apennines belt. Along the fault, in the uppermost crust, the S wave velocity structure is laterally heterogeneous. Right above the hypocenter, we find a 4–6 km thick, very high S wave velocity body (V_s as high as 4.2 km/s) that is absent in the SE portion of the fault, where the earthquake propagated. The high- V_s body is coincident with the area of fewer aftershocks and is anticorrelated with the maximum slip patches of the earthquake, as modeled by differential interferometric synthetic aperture radar (DInSAR) and strong motion data. We interpret this high- V_s body as a high-strength barrier responsible for the high peak ground motion in the near field, observed in the L'Aquila city and surroundings, and for the complexity in the rupture evolution. The retrieved seismic S wave velocity of this body far exceeds common V_s values in the upper crust and it is more compatible with values observed in mafic basement rocks.

Citation: Bianchi, I., C. Chiarabba, and N. Piana Agostinetti (2010), Control of the 2009 L'Aquila earthquake, central Italy, by a high-velocity structure: A receiver function study, *J. Geophys. Res.*, 115, B12326, doi:10.1029/2009JB007087.

1. Introduction

[2] On 6 April 2009, a strong earthquake (M_w 6.3) shocked a densely populated region of the central Apennines, Italy, creating vast damage and loss of cultural sites. Although the Apennines is a site of large destructive earthquakes (see Catalogo Parametrico dei Terremoti Italiani, version 4, INGV, Bologna, <http://emidius.mi.ingv.it/CPTI04/>), the L'Aquila event (Figure 1) developed on a poorly known fault, which was previously identified but thought to be a minor element in accommodating the active extension [Boncio *et al.*, 2004]. Seismologic and geodetic data clearly show that the rupture originated on a semiblind, SW-dipping normal fault [Atzori *et al.*, 2009; Cheloni *et al.*, 2010; Chiarabba *et al.*, 2009a; Cirella *et al.*, 2009; Scognamiglio *et al.*, 2010]. According to geodetic data, the amount of slip at the surface was small (about a few centimeters) [Atzori *et al.*, 2009], while some evidence of surface breaks (5–7 km long) was found, mostly on top of the central portion of the fault [Emergeo Working Group, 2010].

[3] Preliminary results from macroseismic surveys show that the damage was severe and concentrated in the L'Aquila

city and in villages located on the hanging wall of the central portion of the fault. Strong motion records show high peak ground acceleration values at L'Aquila city and a very rapid increase of energy release [Ameri *et al.*, 2009; Çelebi *et al.*, 2010]. Aftershock locations clearly describe the geometry of the fault, but their distribution is nonhomogeneous, with a central portion of the fault where aftershocks are few (Figure 1) [Chiarabba *et al.*, 2009a]. The length of the fault was quantified to be about 16 km [Atzori *et al.*, 2009] and the rupture process highlights an initial slow phase; the more energetic release occurred seconds later [Cirella *et al.*, 2009].

[4] The presence of two permanent broadband stations, AQU and FAGN, located on the hanging wall of the fault (Figure 1) give us the opportunity to define a pseudo 3-D V_s model with high-frequency receiver function (RF) analysis [Ammon, 1991], imaging S wave velocity variations along the fault that can help explain peculiarities in the rupture evolution. The main advantage of this technique is its direct dependence on the S wave velocity, which is a fundamental parameter for the kinematic, and dynamic, modeling of the seismic source [Walters *et al.*, 2009]. The RFs are time series that isolate the P -to- s (Ps) converted phases generated by velocity contrasts present at depth [Ammon, 1991], separating the effects of the structure under the observation point from the source function and the near-source velocity structure [Langston, 1979]. The interpretation of the data set allows us to discriminate between the presence of dipping interfaces [Lucente *et al.*, 2005] and anisotropic layers at depth [i.e.,

¹Istituto Nazionale di Geofisica e Vulcanologia, Centro Nazionale Terremoti, Rome, Italy.

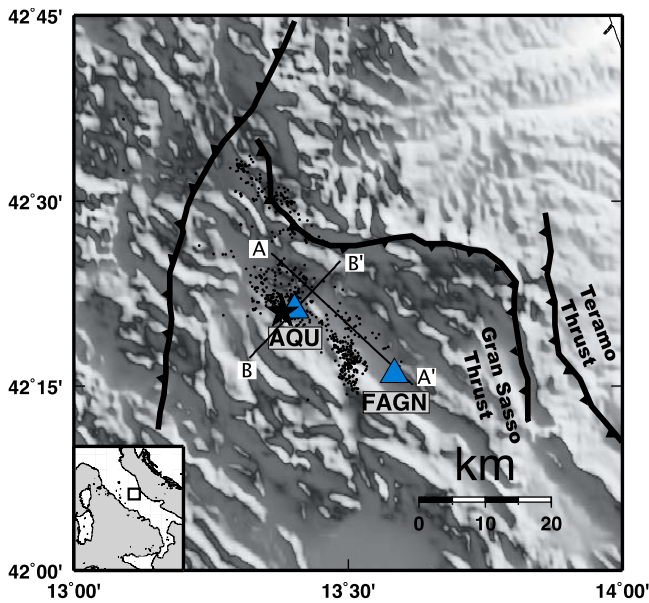


Figure 1. Map of the study area. Blue triangles show the location of the stations, the black star represents the epicenter of the L'Aquila earthquake, and dots are the aftershocks that occurred in the following 2 months. The AA' segment is the hypothesized superficial emergency of the seismogenic fault, and the BB' line is the trace of the downdip profile.

Levin and Park, 1998; Maupin and Park, 2007; Bianchi et al., 2008].

[5] In this study, RFs are obtained by using a 2 Hz low-pass filter, via the method of *Di Bona* [1998], and analyzed by a harmonic decomposition of the RF signal following the work of *Girardin and Farra* [1998]. The data set was inverted by two stochastic methods, first using a transdimensional Metropolis algorithm [*Piana Agostinetti and Malinverno, 2010*] and later with a Monte Carlo sampling technique [*Sambridge, 1999*], to get the 3-D velocity model.

2. Geology and Tectonics of the Area

[6] The two seismic data sets used in this study were recorded at two seismic stations deployed in the central Apennines, which are part of an east-northeast verging fold-and-thrust belt located in the eastern frontal sector of the Apennine-Maghrebien orogen. The whole orogenic system is the result of the collision of the Corsica-Sardinia block (European origin) with the adjacent continental block of Adria during the late Oligocene and Neogene [e.g., *Boccaletti et al., 1971*]. This process followed the consumption and obduction of the Mesozoic Ligure and Ionian domains that were interposed between the two continental blocks [*Finetti, 1985*]. These oceanic derived units, including ophiolitic blocks, outcrop mainly in the Tuscan domain (farther north) [*Boccaletti et al., 1990*] and in the Calabrian arc (farther south) [*Dogliani et al., 1999; Faccenna et al., 2001*], but there is no evidence of these kinds of rocks in the study area. The sedimentary units composing the belt and outcropping in the region consist of sedimentary rocks, a preorogenic passive margin carbonatic sequence overlain by Miocene-Pliocene synorogenic sediments [*Centamore et al., 1986*] (Meso-

Cenozoic sedimentary cover). The older succession is composed of Triassic dolostone and anhydrite that are exposed in the inner sector of the chain. Little is known about the basement, which is not explored in this central part of the Apennines, but the seismic reflection sections deployed farther south (i.e., the CROP 11 line) show a remarkable reflectivity underlying the Mesozoic-Tertiary carbonates, interpreted as a thick Paleozoic-Triassic sedimentary cover of a pre-Cambrian crystalline basement by *Patacca et al. [2008]*.

[7] The thickness of these units, on the basis of well penetration during exploration in surrounding areas, is approximate: 500–6000 m for the siliciclastic synorogenic sediments, 1600–5000 m for the carbonatic sequence, and 1000–4000 m for the dolostone. A general characteristic of the Permian basement underneath the dolostones is its lower seismic velocity with respect to the carbonatic sequence [*Scisciani and Montefalcone, 2006*, and references therein].

[8] Receiver functions for AQU and FAGN stations were previously used to constrain the crustal thickness in the study area [*Piana Agostinetti and Amato, 2009*, and references therein]. The Moho depth values found range between 37 and 42 km. Tomographic images witnessed the alternation of high and low P velocities in the crust [*Di Stefano et al., 2009*].

3. Data and Methods

3.1. Data

[9] We selected good teleseismic events from epicentral distances (Δ) of 30°–105° and magnitude $M_b > 5.5$ recorded at the two stations. Station AQU (Figure 1) belongs to the Mediterranean Network and has been recording since February 1990. Remarkably enough, the station continued operating perfectly during the sequence, even though it is located in the basement of the L'Aquila Castle, which was severely damaged by the event; FAGN is located about 15 km SE of AQU and its recording period started in October 2004 (Figure 1).

[10] The two stations yields a large data set of very high quality RFs: 461 and 201 for AQU and FAGN, respectively, collected between $\Delta = 30^\circ$ and 105° , which fairly cover all the back azimuthal directions (Figure 2). These RF data sets were obtained by deconvolution of the vertical from the horizontal recordings into the radial, transverse, and vertical coordinate system, where the radial (R) is computed along the great circle path between the epicenter and the station, positive away from the source, and the transverse (T) direction is calculated 90° clockwise from R. The deconvolution was performed in the frequency domain [*Langston, 1979; Ammon, 1991*], following the approach proposed by *Di Bona* [1998]. We applied a Gaussian filter ($\alpha = 4$) to limit the frequency band below about 2 Hz [*Langston, 1979*]. The two data sets are displayed in Figure 3 as back azimuthal sweeps. The RFs obtained from the events in Figure 2 have been binned to increase the S/N ratio. Bins shown in Figure 3 are obtained by the stacking of RFs for events occurring in the same area. The spatial filter used to define the events that belong to a single bin is 20° wide in back azimuth (baz) and 40° wide in Δ . In Figure 3, we plot bins computed for an average $\Delta = 90^\circ$ (i.e., Δ for events in the bin ranges between 70° and 105°). Bins are computed using a 50% overlapping

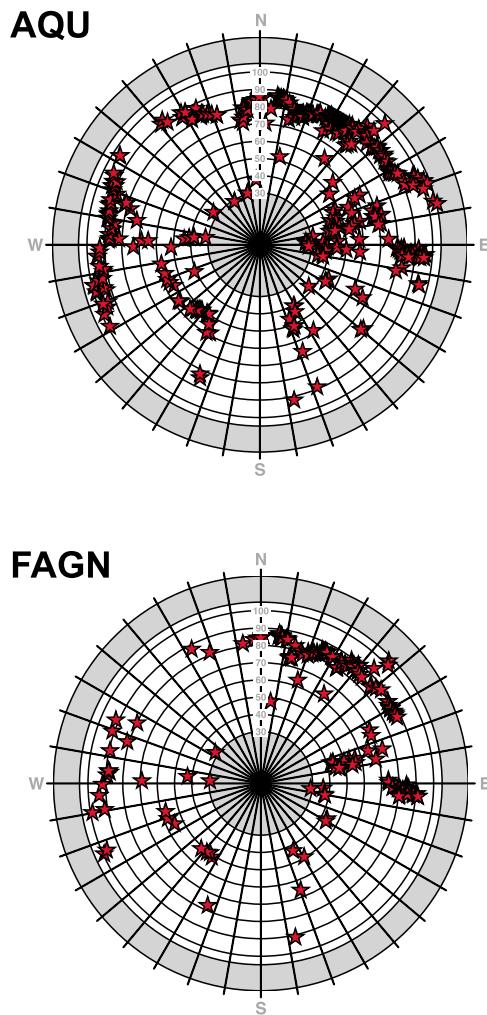


Figure 2. Back azimuthal distribution of the receiver functions obtained by the two stations, (top) AQU and (bottom) FAGN.

scheme (i.e., they are computed every 10° in baz, and a bin shares its events with the two adjacent bins). Bins computed for an average $\Delta = 70^\circ$ (i.e., Δ for events in the bin ranges between 50° and 90°) are included to fill missing baz directions. The good back azimuthal coverage makes 3-D structure modeling beneath the two stations possible from both the radial RF (RRF) and transverse RF (TRF) data sets (Figure 3).

3.2. Data Analysis

[11] We implemented a harmonic angular stacking technique [Girardin and Farra, 1998] to isolate the isotropic structure from the 3-D features. We computed the $k = 0$ harmonic (simple stacking) as the sum of all the RRFs. The $k = 0$ harmonics contain information about the isotropic structure underneath the station (Figure 4). We also calculated the $k = 1$ harmonics, which can be used to reveal features with a periodicity equal to 2π , such as P_S conversions generated from dipping interfaces or anisotropic layers with a dipping symmetry axis [Bianchi et al., 2008]. Both RRFs and TRFs are used to extract the $k = 1$ harmonics (shown in Figure 4), because they generally display a phase shift of $\pi/2$ in back azimuth, so the summation of the $k = 1$ harmonics of

the two components enhances the periodic signal [Shiomi and Park, 2008]. To avoid the use of RFs twice in the analysis, the RFs used to compose Figure 4 have been binned over $\Phi = 10^\circ$ and $\Delta = 20^\circ$, without overlapping with adjacent bins.

[12] The shear velocity model beneath the two stations is investigated through a two-step procedure. First, the $k = 0$ harmonics are used to extract the a posteriori probability density function of the V_s at depth following the approach developed by Piana Agostinetti and Malinverno [2010]. In the second step, we used the recovered isotropic structure to constrain a search for 3-D features such as dipping interfaces or anisotropic layers, which give a satisfactory fit of the $k = 1$ harmonics. The 3-D model is retrieved using a neighborhood algorithm (NA) search [Sambridge, 1999].

3.3. Inversion Method

[13] The RRF inverse problem consists of gaining inferences about the subsurface seismic structure using the RRF time series as observed data. Such inferences can be given in different forms (e.g., a best-fitting seismic model or a probability distribution for some parameters at depth). A single model solution usually fails to catch the obvious non-uniqueness characteristic of the RRF inverse problem [Ammon et al., 1990]. Different techniques have been applied to overcome this problem [e.g., Lodge and Helffrich, 2009]. Here, we adopt a method recently developed by Piana Agostinetti and Malinverno [2010], where a reversible jump Markov chain Monte Carlo (RJMCMC) technique is used to sample the V_s parameter space and to retrieve the a posteriori probability density of the shear velocity beneath a seismic station. The RJMCMC technique does allow one to impose very loose a priori information, such that both the S velocity and the number of seismic discontinuities at depth are considered unknowns. An a posteriori probability distribution (PPD) of the depth of the seismic interfaces beneath the station is computed. Such a distribution broadly indicates how many isotropic layers compose the seismic structure beneath the station and their most probable depths. The a posteriori probability distribution of the S velocity at depth can be used to compute a mean V_s model and to give a measure of the associated errors. We used the $k = 0$ harmonics and the associated standard deviation as observed data for the RJMCMC technique. Prior information about the seismic velocity structure was set as follows. The a priori probability distributions of the S velocity and V_p/V_s are considered Gaussian. For these normal distributions, mean and standard deviation (σ) values are kept constant for V_p/V_s (1.75 and 0.05, respectively), whereas they vary with depth for the V_s to account for large- S velocity variations expected in the shallow crust, where very different lithologies are present (e.g., sediments and carbonates). The number of interfaces is an unknown itself and can vary between 1 and 30. The maximum number of interfaces is given by the resolution of the RF data set. The maximum depth of the interfaces is given by the length of the portion of RF used in the inversion, 0–30 s, and it is fixed to 60 km in this study. The fit between observed and synthetic RF is computed using a classical χ^2 function. Between two interfaces, V_s can display a gradient, whereas V_p/V_s is constant. After a burn-in phase of about 25,000 models, which are discarded, the RJMCMC method was used to sample about 175,000 models, from which we computed the a posteriori probability distributions. We ran

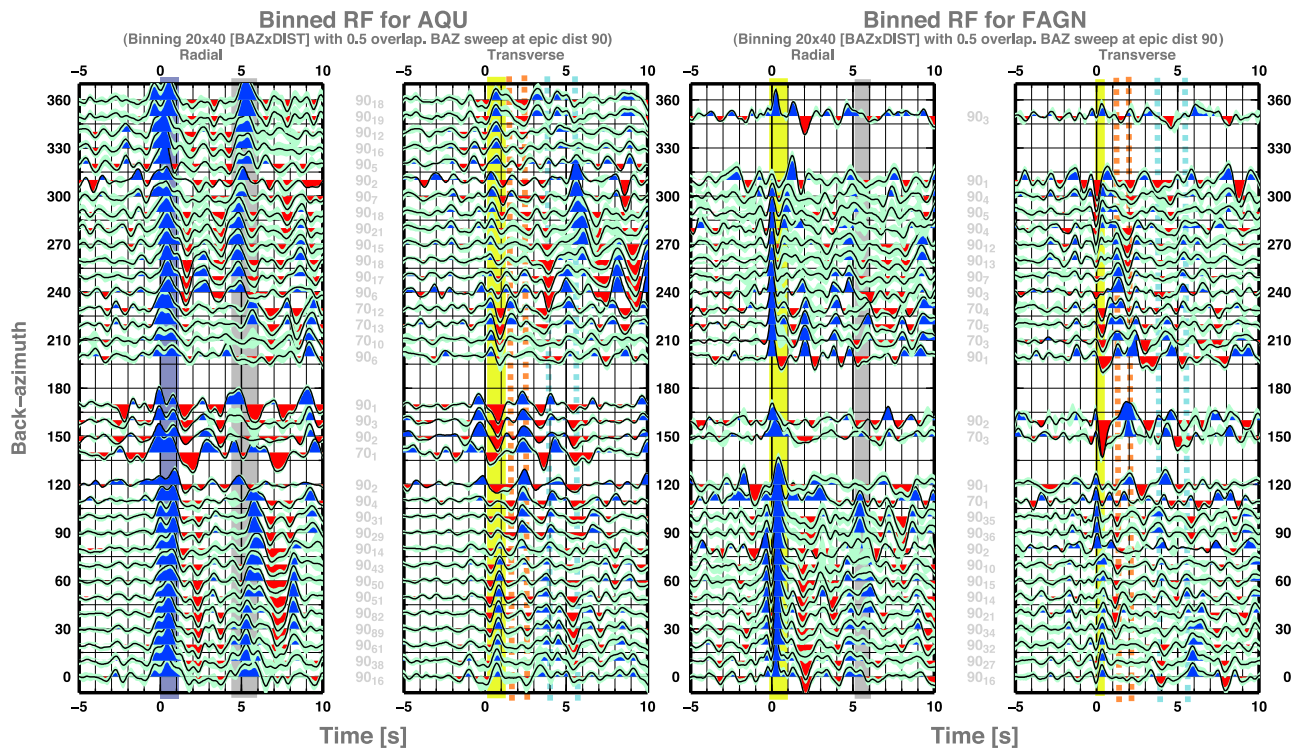


Figure 3. Radial and transverse receiver functions (RFs) for (left) AQU and (right) FAGN as a function of the back azimuth. In the middle of the gathers, large shaded numbers correspond to the reference Δ of the correspondent bin, while small gray numbers denote the number of RFs used to build the respective bin. Colored lines indicate the pulses described in the main text.

95 parallel RJMCMC computations on a linux cluster and obtained an ensemble of about 16×10^6 models. The total CPU time was about 10 h for each station.

[14] The RJMCMC search yields two main results: the PPD of the S velocity at depth, and the distribution of the interface

depth sampled during the chain. We used this information to build a parameter space for the following 3-D V_s modeling, and additional information from the TRF component (pulses in the $k = 1$ diagram), to roughly locate dipping interfaces and anisotropic layers. The mean V_s model from

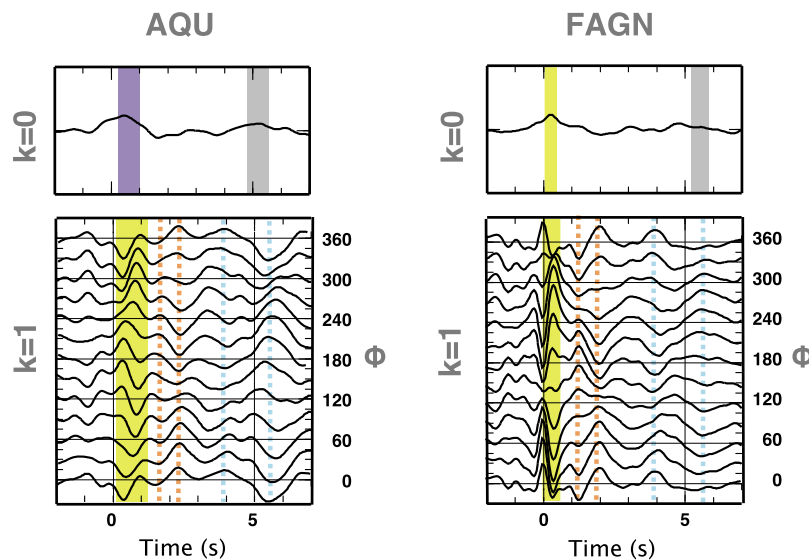


Figure 4. Harmonic analysis for AQU and FAGN data sets, showing (top) the $k = 0$ term as a straight stack of the radial RF, and (bottom) the $k = 1$ term as a summation of RRF and TRF, with a positive shift of 2ϕ . Colors refer to the same features outlined in Figure 3.

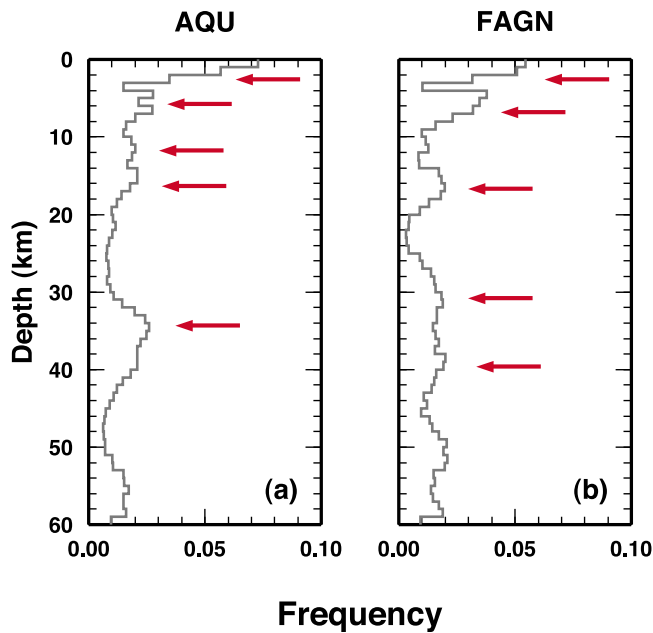


Figure 5. Results from the RJMCMC inversion; histograms of the interface depth sampled during the Markov chain: (a) AQU data set and (b) FAGN data set. The frequency axis represents the ratio between the sampled interfaces at the specific depth and the total of the interfaces sampled during the entire search. Red arrows indicate the highest a posteriori probability for an interface depth.

the RJMCMC search was discretized with reference to the number and depth of the interfaces shown in the histograms of Figure 5. The V_s models were divided into layers with uniform velocity, and 3-D values were assigned to perform the NA search following the work of *Sambridge* [1999]. This technique uses the properties of Voronoi cells to drive the search into a multidimensional parameter space, with the aim of finding an ensemble of models with acceptable data fit. We generated 1000 initial random samples inside the parameter space, and the four cells with the lowest misfit were resampled to produce 20 new samples. This process was repeated 500 times, for a total of 11,000 models explored for each station. The best fit model is interpreted as representative of the ensemble. Synthetics are calculated using the RAYSUM code [*Frederiksen and Bostock*, 2000] that models the propagation of a plane wave in dipping and anisotropic structures. Anisotropy was modeled as hexagonal with a unique axis of symmetry, because this is the most common fabric of rocks that is easily reproducible [*Levin and Park*, 1998]. In a hexagonal system, there is one main axis of symmetry; in the plane perpendicular to the axis of symmetry, every direction is indistinguishable. P wave propagation along the axis of symmetry can be either faster or slower than that in the perpendicular plane. If the P wave propagation is fast, the axis of symmetry is considered to be fast, and this is also called positive anisotropy. If the P wave propagation is slow, the symmetry axis is considered to be slow (negative anisotropy) [*Savage*, 1998]. In the considered models, P and S anisotropy parameters are set to be equal to reduce the nonuniqueness of the calculation. Dipping interfaces and anisotropic layers produce similar signals that are difficult

to distinguish [*Savage*, 1998; *Bianchi et al.*, 2008]. Thus, we use dipping interfaces to reproduce 3-D features in the very shallow crust, because a small dip of discontinuities can be generated by the Apennines faults and folded structures [see also *Lucente et al.*, 2005]. Conversely, we prefer to use anisotropic layers at greater depths, because highly dipping, sharp structures are rare in the middle and lower crust [*Sherrington et al.*, 2004]. The retrieved models are just a simplification of the structure beneath, which is much more complex and not simply due to planar planes or hexagonal anisotropy. Although it is an oversimplification of the real geometry, the model is the simplest that fits the observed RRF and TRF data.

4. Results

4.1. AQU

[15] The AQU data set shows the arrival of several phases in the first 5 s, generated by crustal heterogeneities (Figure 3). The first second of the R gather is composed of two positive pulses, that is, the direct P and a first P_s phase (indicated by a violet bar). The time delay of the P_s phase with respect to the direct P displays a clear dependence on back azimuth, reaching its maximum value (about 1.0 s) for 120° – 150° back azimuth directions. The T signal is small in the same time window but shows a “doublet” (i.e., a positive pulse followed by a negative one with the same amplitude), also called a “derivative pulse” (outlined by two yellow dotted lines), which inverts its polarity in the same back azimuth direction. The deeper features consist of two negative pulses centered at 2 and 3.5 s, evidence of a V_s decrease, and is associated with energy in the T component (marked by orange lines). An extremely strong positive pulse at 5–5.5 s on the R gather (highlighted by a gray line) is associated with a double pulse reversing at about 180° direction on the T component (light blue dotted lines). The RRFs and TRFs present comparable amplitudes, suggesting the presence of 3-D features such as dipping interfaces and anisotropic layers in the crust. In the velocity model recovered by the RJMCMC inversion, the V_s abruptly reaches very high values (more than 4 km/s) at depths shallower than 10 km (Figure 6). In the middle crust, a low V_s layer is present (V_s of about 3.1 km/s). At greater depth, V_s continuously increases to velocities characteristic of the mantle, at a depth of about 41 km. The observed and synthetic data are shown in Figure 7a. The presence of the isotropic interfaces is highlighted by the histogram in Figure 5a. We identify at least two shallow discontinuities in the first 2 km depth, and other interfaces located at about 5, 11, 15, and 35 km depth. The 3-D information visible in the $k = 1$ data set (Figure 4) led us to introduce more layers in the parameter space for the NA search, because four phases are localized during the first second, at 1.5–2.5 s and 3.9–5.5 s. The parameter space for station AQU is constructed by grouping together the described information deduced from both the $k = 0$ and $k = 1$ data sets: six isotropic discontinuities, two of which are coincident with the anisotropic signal, and one additional anisotropic feature (at 3.9 s). Two further interfaces are added to reproduce the large Moho pulse observed at 5.5 s in the $k = 0$ diagram (Figure 4), which suggest a layered structure for the basement. The parameter space has a total of 10 layers.

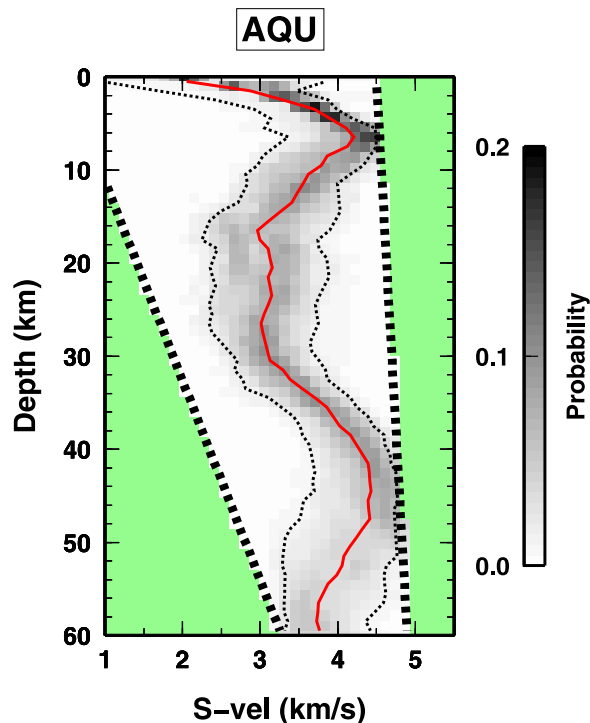


Figure 6. Results from the RJMCMC inversion, for station AQU. Posterior sampling of the V_s parameter at depth. Shading represents the posterior probability density at different depths for the S velocity. Thick dotted lines indicate the boundaries of the parameter space for the S velocity parameter. The mean value of V_s at each depth level is shown as a red line. Thin dotted lines indicate the $\pm 2\sigma$ deviation for the V_s parameter.

[16] Figure 8 shows the best fit model of the NA search, and parameters of the best fit model are reported in Table 1. In the upper crust (0–10 km depth), we find three features: (1) a shallow, 1 km thick, low- V_s layer ($V_s = 1.5$ km/s), interpreted as sediments of the L'Aquila basin; (2) a 2 km thick, $V_s = 2.9$ km/s layer, interpreted as a layer of Meso-Cenozoic limestones; and (3) a 7 km thick, very high velocity layer (V_s reaching about 4.2 km/s) whose top is inclined toward the SE. The nature of this layer is not easily explainable, because the overall thickness and velocities are excessive for carbonate or dolomitic rocks. We suggest the hypothesis that such high velocities are related to a mafic basement (i.e., exhumed deep crust and mantle rocks) obducted during the collision and dragged into the sedimentary pile.

[17] In the middle crust, we find two main layers: (1) a 5 km thick anisotropic layer with $V_s = 3.4$ km/s and an anisotropic slow axis that trends NE 200° and plunges 25° (we interpret this layer as a second deep unit composed of the Adria Mesozoic cover) and (2) a 5 km thick low-velocity layer (V_s about 3.1 km/s), likely a fluid-filled weak layer forming the decollement above which the Apenninic wedge was stacked.

[18] In the lower crust, we find a unit that can be associated to the underthrusting Adria lithosphere: a layer at depth between 20 and 24 km, interpretable as metamorphosed remnants of the Adria sedimentary cover ($V_s = 3.4$ km/s), and a 17 km thick layered and anisotropic basement in which about 9% anisotropy is present with a symmetry axis trending

NE 174° and plunging 57° . Velocities increase and reach mantle values at 41 km depth. We interpreted this feature as due to the Adria layered lower crust under-thrusting the belt.

4.2. FAGN

[19] In the FAGN data set, the first pulse is very sharp and picked at about 0.5 s (outlined by a yellow line in Figure 3), displaying a move out with maximum delay time toward the NE. The deeper features consist of two negative pulses at 2 and 3.5 s and a positive pulse at about 5 s (marked by a gray line) on the R gather, while the T gather shows, in the first 0.5 s, a phase reversing in the NE direction, some energy clustered around 2 s reversing southward (orange dotted lines), and a double pulse reversing in the S direction and located at 3.5 and 5.5 s (light blue dotted lines). The RRFs and TRFs present comparable amplitudes highlighting the presence of strong 3-D features as dipping interfaces and anisotropic layers inside the crust (these features are highlighted as for the AQU data set). In the shallow structure recovered by the RJMCMC inversion (Figure 9), the V_s values slightly increase, keeping average shallow crust values. At about 15 km depth, a low- V_s layer (V_s of about 3.0 km/s) is found. At greater depth, FAGN shows a slight and constant increase up to mantle velocities, reached at about 40 km depth. The observed and synthetic data sets are shown in Figure 7b.

[20] We parameterize the model for the NA search, including both isotropic interfaces located at about 2, 6, 10,

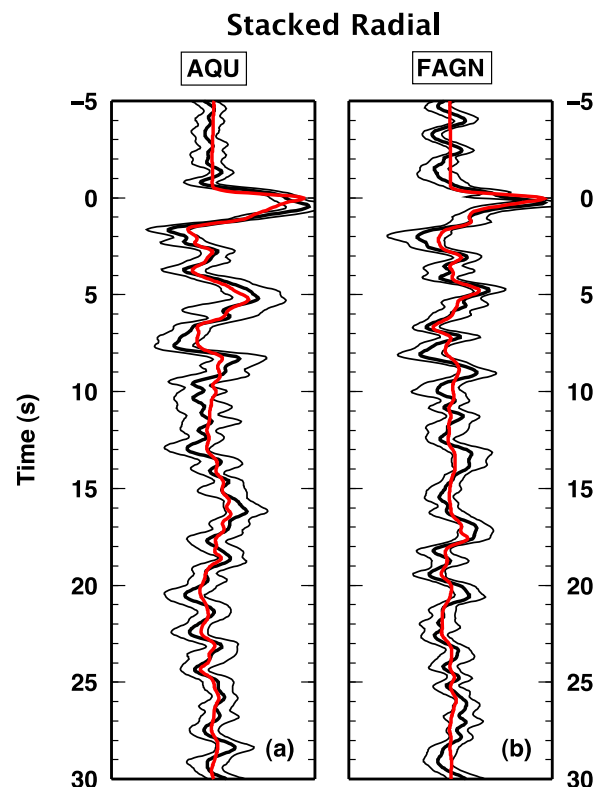


Figure 7. Results from the RJMCMC inversion: (a) AQU data set and (b) FAGN data set. Black thick and thin lines show observed stacked radial RF (or $k=0$) and $\pm 2\sigma$ deviation. Red lines indicate the mean synthetic RF.

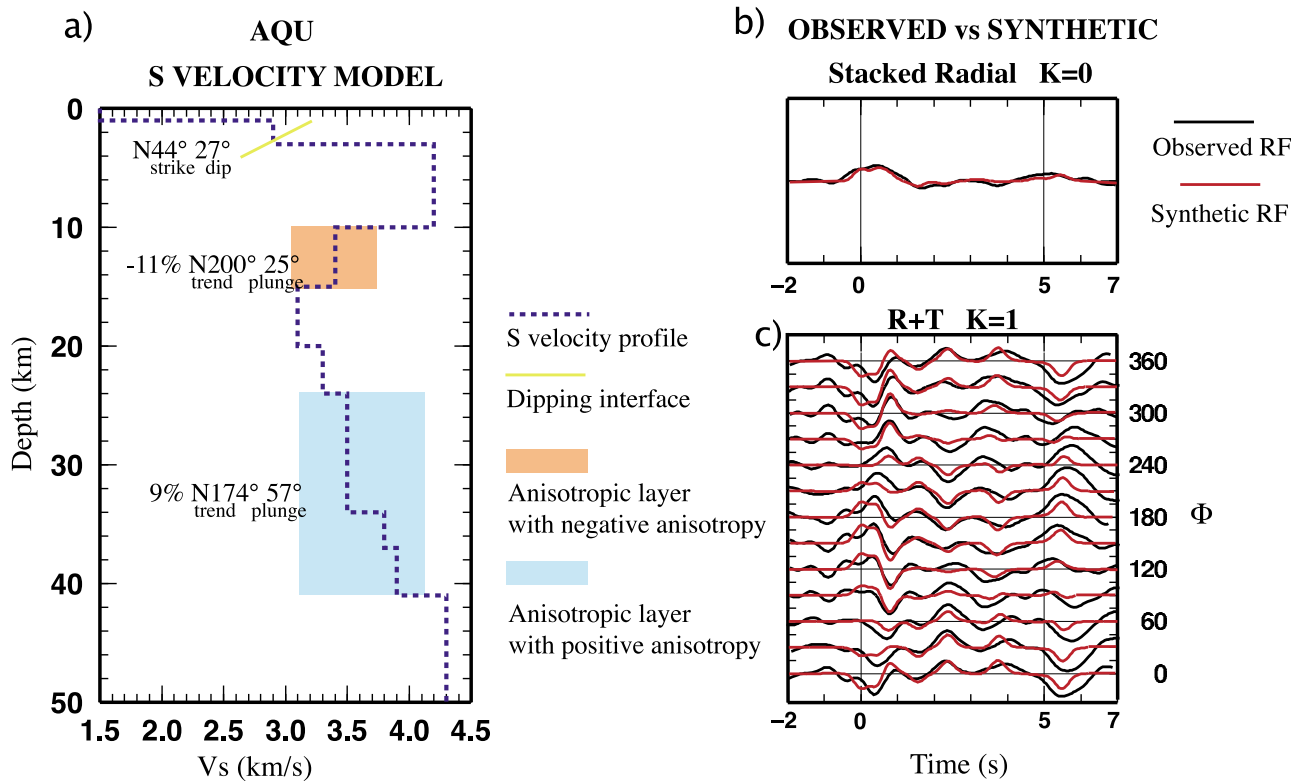


Figure 8. (a) S velocity model (blue dashed line) for station AQU; the shallow inclined interface is represented by a yellow line, and the anisotropic layers are represented as colored rectangles: orange for the shallow anisotropic layer with slow symmetry axis, and light blue for the deep layer with fast symmetry axis. (b, c) Observed (black lines) versus synthetic (red lines) RFs for station AQU. Figure 8b shows the stacked radial as the $k = 0$ term of the harmonic analysis. Figure 8c shows the summation of radial and transverse RFs, as the $k = 1$ term of the harmonic analysis.

16, 30, and 40 km depth (Figure 5b), and the 3-D features used to model the signals at 0.5 s, 1.2–2 s, and 3.9–5.5 s, visible in the $k = 1$ gather (outlined by colors as in Figure 4). The recovered S velocity model (Figure 10) is the best fit model of the search, and its parameters are summarized in Table 2.

[21] The upper crust (0–8 km depth) consists of (1) a slow V_s (1.7 km/s) shallow layer of synorogenic sediments, (2) an inclined interface striking $N 334^\circ$ and plunging 20° , and (3) two layers with relatively high V_s velocity ($V_s < 3.7$ km/s), interpreted as limestone and dolomitic rocks of the Mesozoic cover.

Table 1. Velocity Model for AQU as in Figure 8

Depth (km)	V_s (km/s)	P and S Aniso (%)	Trend	Plunge	Strike	Dip
1	1.5					
3	2.9					
10	4.2				44	27
15	3.4	-11	200	25		
20	3.1					
24	3.3					
34	3.5	9	174	57		
37	3.8	9	174	57		
41	3.9	9	174	57		
Half-space	4.3					

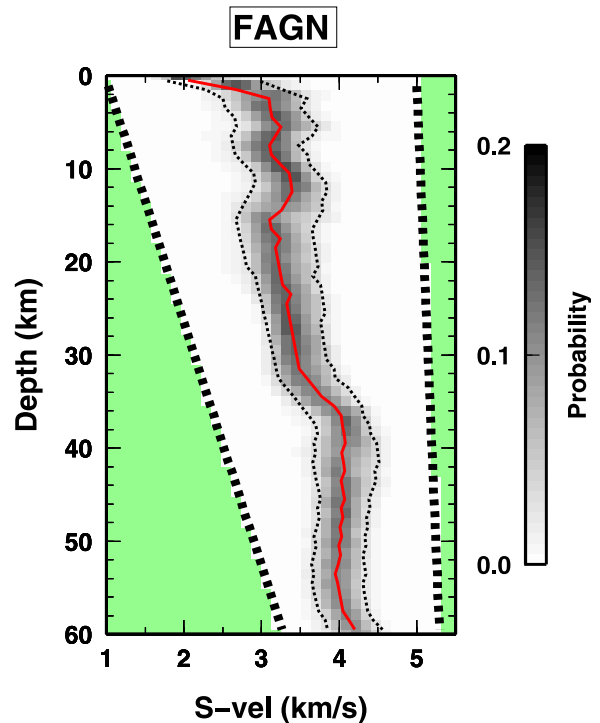


Figure 9. Results from the RJMCMC inversion. Same as in Figure 6, but for station FAGN.

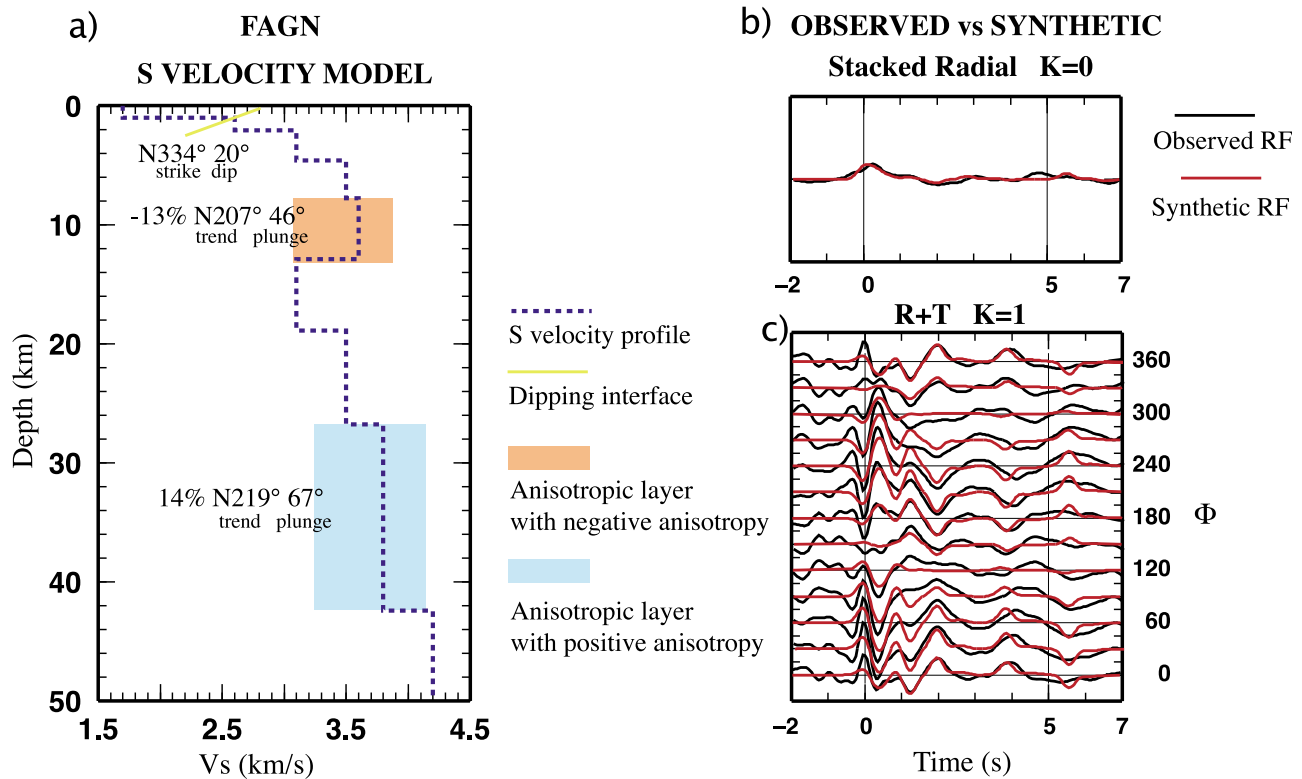


Figure 10. (a) S velocity model for station FAGN. (b, c) observed (black lines) versus synthetic (red lines) RFs for station FAGN, as in Figure 8.

[22] Underneath FAGN, V_s as high as 4.2 km/s are not found; the higher values are 3.7 km/s.

[23] The middle crust is composed of two layers that are comparable with those modeled at station AQU: (1) a high- V_s (3.6 km/s), 5 km thick, anisotropic layer, with -13% P and S anisotropy for which the symmetry axis trends N 207°, with 46° plunge and (2) a slow- V_s (3.0 km/s), 6 km thick layer for which the bottom is at about 18 km depth. Notably, these two latter layers display the same characteristics seen in the AQU middle crust.

[24] In the lower crust, the deep unit associated with the under-thrusting Adria has two main features: (1) a relatively high V_s (3.5 km/s), 8 km thick, isotropic layer down to 26 km depth and (2) an anisotropic 16 km thick layer that lies above a Moho modeled at 42 km depth. It shows strong anisotropy (14% ΔV_s), with a fast symmetry axis oriented at N 219° plunging 67°. The S wave velocity is equal to 3.8 km/s and does not show jumps, such as those found in station AQU. We interpret this layer as the basement of Adria.

5. Discussion

[25] The geology and structure of central Apennines were intensively studied with surface data [e.g., Bigi *et al.*, 1999] and, to some extent, by seismic reflection profiles [Mostardini and Merlini, 1986; Scisciani and Montefalcone, 2006; Patacca *et al.*, 2008]. The central Apennines has a higher elevation than other parts of the Apennines and displays a difference between the regional divide and the culmination of topography, suggesting a dynamic support to the topography [D'Agostino and McKenzie, 2000].

Tomographic images reveal a large area in the lower crust and uppermost mantle with very low P wave velocities [Di Stefano *et al.*, 2009; Chiarabba *et al.*, 2009b], interpreted as a window of the Apennines slab. Recent RF studies, computed with mostly temporary, short-lived seismic stations [Di Bona *et al.*, 2008; Di Luzio *et al.*, 2008], commonly identify the presence of a thick crust (more than 40 km), but results leave open quite different interpretations and geodynamic models. All previous RF studies modeled only the simple 1-D structure, focusing on the Moho depth and neglecting all the energy present in the T component and the clear move out of converted pulses observable in the R component (see Figure 3). In this study, we analyzed the most complete data set for AQU and FAGN stations, almost 20 and 5 years of data, respectively, modeling the 3-D structure with a good fit of both R and T components. The simultaneous modeling of 1-D and 3-D features is a key to obtaining

Table 2. Velocity Model for FAGN as in Figure 10

Depth (km)	V_s (km/s)	P and S Aniso (%)	Trend	Plunge	Strike	Dip
1	1.7					
2	2.6				334	20
5	3.1					
8	3.5					
13	3.6	-13	207	46		
19	3.1					
27	3.5					
42	3.8	14	219	67		
Half-space	4.2					

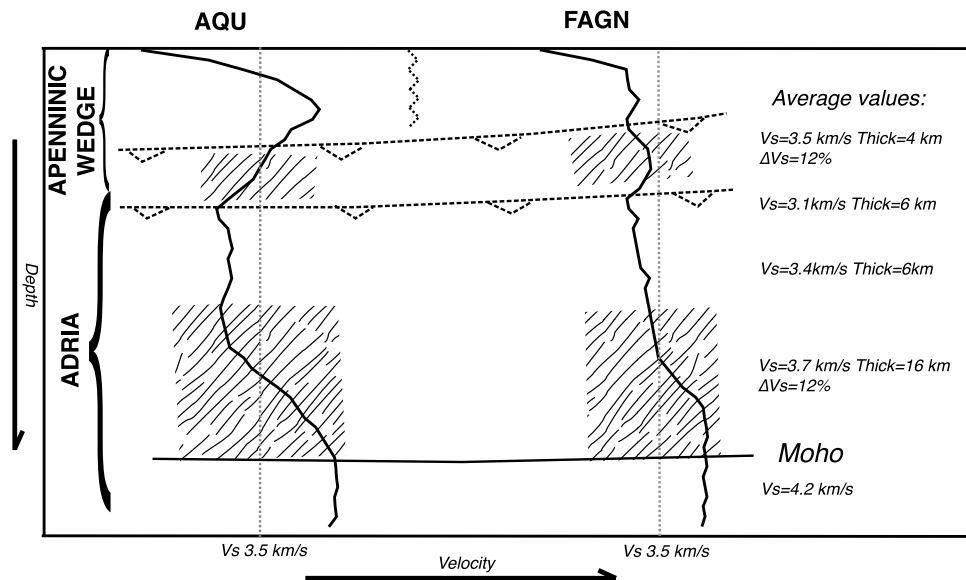


Figure 11. Correlation of the common features of the models obtained for AQU and FAGN. The lined boxes represent the anisotropic portions of the crust as recovered by the 3-D inversions. The shallow anisotropic layer delineates the bottom of the Apenninic wedge speculatively bounded by the two main thrusts of the area. On the right, the average values for V_s and anisotropy percentage coming from the 3-D models are shown.

reliable features in complex areas, whereas neglecting 3-D features may lead to local minima of the solution [Bianchi *et al.*, 2008]. The 3-D models for the two close stations reveal strong differences for the shallow crust, whereas deeper features are similar. The difference of the AQU and FAGN models in the upper crust implies that the piled-up Apenninic wedge, thrust over the west-dipping Adria lithosphere, is strongly heterogeneous.

5.1. Regional Structure of the Crust

[26] The similarity in the deeper part of the V_s models indicates a common regional structure, upon which the thrust nappes developed. For both stations, the structure of the eastward thrusts and the underlying Adria lithosphere is consistent and well defined. The deep unit (ADRIA in Figure 11) has a total crust thickness of about 20–25 km, which agrees with the crust thickness observed at stations OFFI, FRES, and TRTR, located in the external area, before the flexing of Adria [Piana Agostinetti and Amato, 2009]. On top of the under-thrusting Adria, two thrust units forming the Apenninic wedge were stacked, involving both the limestone Meso-Cenozoic cover and part of the underlying basement (Figure 11). The shallowest thrust is reasonably coincident with the Gran Sasso structure (Figure 1), whereas the deeper thrust can be associated to a more external thrust [Bigi *et al.*, 1999]. The decollement levels are tentatively located between the anisotropic shallow layer and the negative V_s gradients between approximately 10 and 18 km depth, suggestive of a weak level or fluid-filled zone, and the location of the intense thrusting [Chiarabba *et al.*, 2009b] (Figure 11). The SSW-dipping observed anisotropy agrees with the geometry of the thrust-and-fold Apennines belt, where the deformations are caused by cracks and microcracks

[Kaneshima *et al.*, 1988] formed during the emplacement of the thrust unit.

5.2. Seismogenic Layer

[27] The upper structure recovered for the two stations is considerably different, suggesting that the units piled up in thrusts have strong lateral variations caused by either the complex geometry of the thrust system or lateral variations of the pre-Mesozoic basement. Underneath AQU, V_s abruptly reaches very high values ($V_s > 4$ km/s, Figure 8), whereas the V_s values at FAGN are smaller and within limits usually observed for carbonate rocks (Figure 10). Such high V_s bodies have not been found previously in this zone, nor have gravimetric or magnetic anomalies been detected with such detail until now. The presence of this structure is strongly constrained from our inversions, and it is very localized because it is present underneath the AQU station and absent beneath the FAGN station. Our hypothesis is that some portions of the mafic basement obducted during the collision of the two plates may have been detached and included in the thrust pile.

[28] The presence of this localized and laterally discontinuous high- V_s body in the upper crust may have significantly influenced the generation and propagation of the 2009 L'Aquila earthquake rupture. The body is in fact located along the fault, surrounded by the maximum slip patches observed by Cirella *et al.* [2009]. In Figure 12, we compare the location of the high- V_s body with the slip on the fault plane, for which emersion is line AA' in Figure 1, and the aftershocks occurred during the first 2 months [Chiarabba *et al.*, 2009a]. The main shock rupture started at the base of the high- V_s body and propagated through the body. We computed synthetic tests trying to model the conversion as due to a thin high- V_s layer coincident with the fault (high-

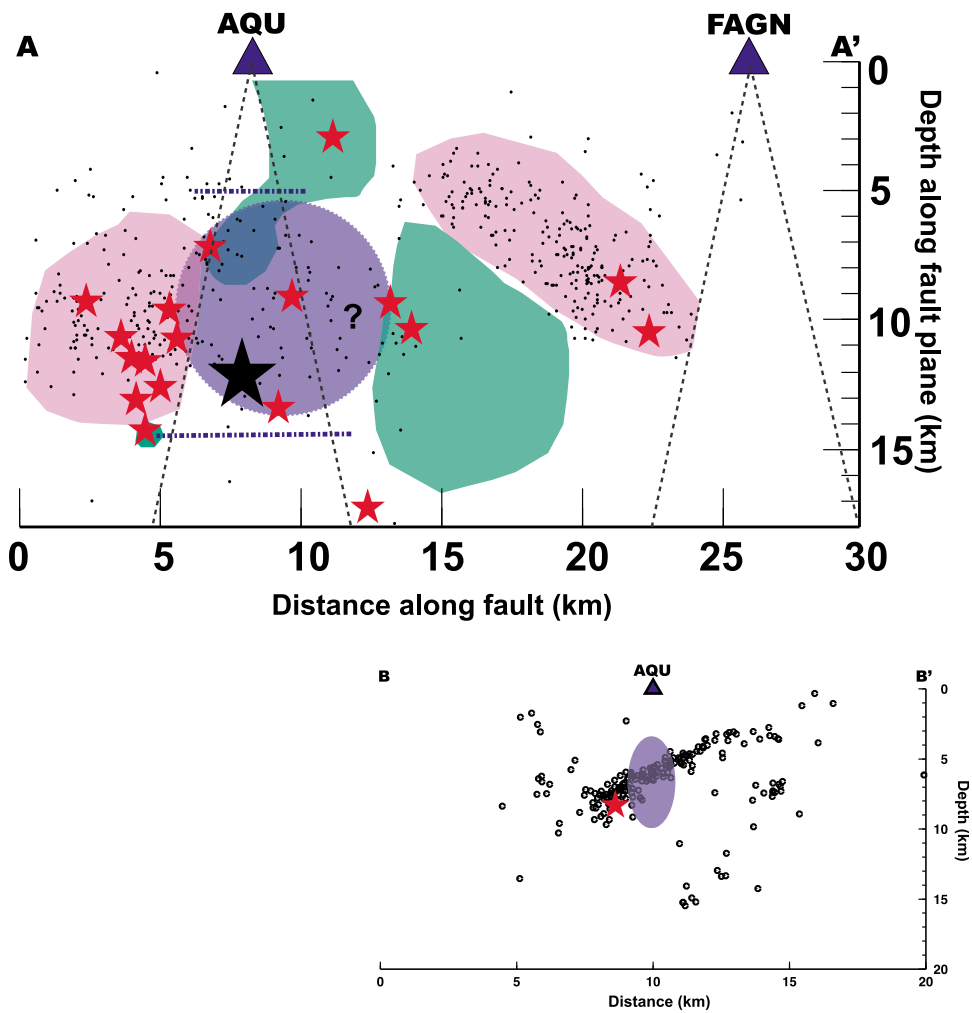


Figure 12. (AA') Fault plane showing the location of the V_s barrier (violet area), the maximum slip patches (green area, as retrieved by *Cirella et al.* [2009]) and the compliant area (pink area, from the aftershocks distribution located by *Chiarabba et al.* [2009a]). The black star is the main shock, red stars are the $M > 4$ aftershocks, and black dots are the smaller aftershocks, projected on the fault plane. Triangles represent the projection of the seismic station on the fault trace, and the dotted gray lines delimit their illumination area. Dotted blue lines represent the top and the bottom of the high- V_s body detected under station AQU projected on the fault plane. (BB') down-dip (vertical) section showing the relationship between the aftershock distribution (black dots) and the location of the high- V_s body (violet ellipse). The red star represents the location of the main shock.

strength material that clogs the fault), finding patterns on the R and T components different from those observed. Although the resolution of teleseismic waveforms is limited (hundreds to thousands of meters), we hypothesize that the high- V_s material is present on both sides of the fault.

[29] The main shock signal during the first seconds, as observed by both close and distant stations [*Chiarabba et al.*, 2009a], is emergent. After about 1 s, the high-energy pulse occurred, suggesting a rapid acceleration of the rupture, with a short high-frequency radiation and very high peak ground acceleration for a M_w 6.3 event, as observed by strong motion recordings [*Ameri et al.*, 2009; *Çelebi et al.*, 2010]. The initial slow rupture, whose hypocenter is at about 10 km depth [*Chiarabba et al.*, 2009a], probably originated within the high- V_s body. The lateral extent of this body to the south, presumably small because it is absent beneath the FAGN

station, is anticorrelated with the area with the largest coseismic slip as modeled by differential interferometric synthetic aperture radar (DInSAR) [*Atzori et al.*, 2009] and strong motion data [*Cirella et al.*, 2009]. We interpret the high- V_s body as a strong fault section acting as a high-strength barrier [*Dunham et al.*, 2003], with a slip deficit during the event. The majority of aftershocks originated outside this high- V_s zone, delineating the compliant region around the main asperity. Its localization may account for the repetition of similar earthquakes, in agreement with the similar damages observed by macroseismic studies for the 2009 and the 1461 earthquakes (see *Catálogo Parametrico dei Terremoti Italiani*, version 4, INGV, Bologna, <http://emidius.mi.ingv.it/CPTI04/>). Finally, the very low V_s shallowest layer found underneath AQU and FAGN stations indicates that Quaternary sediments are very thick (around 1 km) beneath

the Aquila basin and may account for the local amplification of ground motion during the earthquake.

6. Conclusions

[30] We find an exceptionally high velocity body ($V_s > 4.0$ km/s) along the fault ruptured during the 2009 L'Aquila earthquake. This body is laterally not continuous and its extent is anticorrelated with the area of maximum slip and sparse aftershocks, as observed by geodetic and seismologic data. The nature of this body is speculative because such high velocities are consistent with deep crust or upper mantle rocks and are over the limit of carbonate rocks ($V_s < 3.7$ km/s). Independent geophysical data are required to fully assess which type of rocks forms the lower part of the thrust unit. Whatever the rock type, we interpret the high V_s as a strong portion of the fault with insignificant slip during the event. This high-strength barrier concentrated energy and produced the strong pulse observed at the stations located around L'Aquila. The presence of such high velocities should be taken into account while modeling the kinematics or dynamics of the L'Aquila seismic source. Moreover, its presence probably affected the displacement of the Gran Sasso thrust, which is partially E-W oriented while the surrounding structures display the NW-SE Apenninic characteristic vergence. Future directions will be the analysis of RFs from the temporary stations installed in the epicentral region to better confine the extent of the high- V_s body.

[31] **Acknowledgments.** I.B. is supported by DPC-S1_UR02.02 and INGV, CNT, N.P.A. is supported by project Airplane (funded by the Italian Ministry of Research, project RBPR05B2ZJ_003). Thanks go to Antonella Cirella and Alberto Michelini for helpful discussions. We thank Massimo Di Bona for providing the software for RF computation. We thank the anonymous reviewers and the Editor for the suggestions that they gave to improve our manuscript; particular thanks are addressed to the Associate Editor who made a deep revision of the manuscript for its better comprehension. GMT [Wessel and Smith, 1991] was used for developing figures.

References

- Ameri, G., et al. (2009), The 6 April 2009 M_w 6.3 Aquila (central Italy) earthquake: Strong-motion observations, *Seismol. Res. Lett.*, *80*(6), 951–966, doi:10.1785/gssrl.80.6.951.
- Ammon, C. (1991), The isolation of receiver effects from teleseismic p waveforms, *Bull. Seismol. Soc. Am.*, *81*, 2504–2510.
- Ammon, C., G. E. Randall, and G. Zandt (1990), On the non-uniqueness of receiver function inversions, *J. Geophys. Res.*, *95*, 15,303–15,318.
- Atzori, S., et al. (2009), Finite fault inversion of DInSAR coseismic displacement of the 2009 L'Aquila earthquake (central Italy), *Geophys. Res. Lett.*, *36*, L15305, doi:10.1029/2009GL039293.
- Bianchi, I., N. Piana Agostinetti, P. De Gori, and C. Chiarabba (2008), Deep structure of the Colli Albani volcanic district (central Italy) from receiver functions analysis, *J. Geophys. Res.*, *113*, B09313, doi:10.1029/2007JB005548.
- Bigi, S., F. Calamita, G. Cello, E. Centamore, G. Deiana, W. Paltrinieri, P. Pietrantonio, and M. Ridolfi (1999), Tectonics and sedimentation within a Messinian foredeep in the central Apennines, Italy, *J. Pet. Geol.*, *22*(1), 5–18.
- Boccaletti, M., P. Elter, and G. Guazzane (1971), Plate tectonic models for the development of the western Alps, and northern Apennines, *Nat. Phys. Sci.*, *234*, 108–110.
- Boccaletti, M., F. Calamita, G. Deiana, R. Gelati, F. Massari, G. Moratti, and F. Ricci Lucchi (1990), Migrating foredeep-thrust belt system in the northern Apennines and southern Alps, *Palaeogeogr. Palaeoclimatol. Palaeoecol.*, *77*, 3–14.
- Boncio, P., G. Lavecchia, and B. Pace (2004), Defining a model of 3D seismogenic sources for seismic hazard assessment applications: The case of central Apennines (Italy), *J. Seismol.*, *8*, 407–425.
- Çelebi, M., et al. (2010), Recorded motions of the M_w 6.3 April 6, 2009 L'Aquila earthquake and implications for building structural damage, earthquake spectra, *Earthquake Spectra*, *26*(3), 651–684.
- Centamore, E., G. D. nad A. Micarelli, and M. Potetti (1986), Il Trias—Paleogene delle Marche, *Stud. Geol. Camerti*, spec. vol., 9–27.
- Cheloni, D., et al. (2010), Coseismic and initial postseismic slip of the 2009 M_w 6.3 L'Aquila earthquake, Italy from GPS measurement, *Geophys. J. Int.*, *181*(3), 1539–1546.
- Chiarabba, C., et al. (2009a), The 2009 L'Aquila (central Italy) M_w 6.3 earthquake: Mainshock and aftershock, *Geophys. Res. Lett.*, *36*, L18308, doi:10.1029/2009GL039627.
- Chiarabba, C., P. De Gori, and F. Speranza (2009b), Deep geometry and rheology of an orogenic wedge developing above a continental subduction zone: Seismological evidence from the northern-central Apennines (Italy), *Lithosphere*, *1*(2), 95–104.
- Cirella, A., A. Piatanesi, M. Cocco, E. Tinti, L. Scognamiglio, A. Michelini, A. Lomax, and E. Boschi (2009), Rupture history of the 2009 L'Aquila (Italy) earthquake from non-linear joint inversion of strong motion and GPS data, *Geophys. Res. Lett.*, *36*, L19304, doi:10.1029/2009GL039795.
- D'Agostino, N., and D. McKenzie (2000), Convective support of long-wavelength topography in the Apennines, *Terra Nova*, *11*, 234–238.
- Di Bona, M. (1998), Variance estimate in frequency-domain deconvolution for teleseismic receiver function computation, *Geophys. J. Int.*, *134*, 634–646.
- Di Bona, M., F. P. Lucente, and N. Piana Agostinetti (2008), Crustal structure and Moho depth profile crossing the central Apennines (Italy) along the N42° parallel, *J. Geophys. Res.*, *113*, B12306, doi:10.1029/2008JB005625.
- Di Luzio, E., G. Mele, M. M. Tiberti, and G. P. Cavinato (2008), Moho deepening and shallow upper crustal delamination beneath the central Apennines, *Earth Planet. Sci. Lett.*, *280*, 1–12, doi:10.1016/j.epsl.2008.09.018.
- Di Stefano, R., E. Kissling, C. Chiarabba, A. Amato, and D. Giardini (2009), Shallow subduction beneath Italy: Three-dimensional images of the Adriatic-European-Tyrrhenian lithosphere system based on high-quality P wave arrival times, *J. Geophys. Res.*, *114*, B05305, doi:10.1029/2008JB005641.
- Doglionni, C., P. Harabaglia, S. Merlini, F. Mongelli, A. Peccerillo, and C. Piromallo (1999), Orogens and slabs vs their direction of subduction, *Earth Sci. Rev.*, *45*, 167–208.
- Dunham, E. M., P. Favreau, and J. M. Carlson (2003), A supershear transition mechanism of cracks, *Science*, *299*, 1557–1559.
- Emergeo Working Group (2010), Evidence for surface rupture associated with the M_w 6.3 L'Aquila earthquake sequence of April 2009 (central Italy), *Terra Nova*, *22*, 43–51, doi:10.1111/j.1365-3121.2009.00915.x.
- Faccenna, C., T. W. Becker, F. P. Lucente, L. Jolivet, and F. Rossetti (2001), History of subduction and back-arc extension in the central Mediterranean, *Geophys. J. Int.*, *145*, 809–820.
- Finetti, I. R. (1985), Structure and evolution of the central Mediterranean (Pelagian and Ionian seas), in *Geological Evolution of the Mediterranean Basin*, edited by D. J. Stanley and F.-C. Wezel, pp. 215–230, Springer-Verlag, New York.
- Frederiksen, A. W., and M. G. Bostock (2000), Modeling teleseismic waves in dipping anisotropic structures, *Geophys. J. Int.*, *141*, 401–412.
- Girardin, N., and V. Farra (1998), Azimuthal anisotropy in the upper mantle from observation of P -to- S converted phases: Application to southeast Australia, *Geophys. J. Int.*, *133*, 615–629.
- Kaneshima, S., M. Ando, and S. Kimura (1988), Evidence from shear-waves splitting for the restriction of seismic anisotropy to the upper crust, *Nature*, *335*, 627–629.
- Langston, C. A. (1979), Structure under Mount Rainier, Washington, inferred from teleseismic body waves, *J. Geophys. Res.*, *84*(B9), 4749–4762.
- Levin, V., and J. Park (1998), P - SH conversions in layered media with hexagonally symmetric anisotropy: A cookbook, *Pure Appl. Geophys.*, *151*(2–4), 669–697.
- Lodge, A., and G. Helffrich (2009), Grid-search inversion of teleseismic receiver functions, *Geophys. J. Int.*, *178*, 513–523.
- Lucente, F. P., N. Piana Agostinetti, M. Moro, G. Selvaggi, and M. Di Bona (2005), Possible fault plane in a seismic gap area of the southern Apennines (Italy) revealed by receiver functions analysis, *J. Geophys. Res.*, *110*, B04307, doi:10.1029/2004JB003187.
- Maupin, V., and J. Park (2007), Theory and observations: Wave propagation in anisotropic media, in *Treatise on Geophysics, Seismology and Structure of the Earth*, vol. 1, edited by B. Romanowicz and A. Dziewonski, pp. 289–321, Elsevier, New York.
- Mostardini, E., and S. Merlini (1986), Appennino centro-meridionale: Sezioni geologiche e proposta di modello strutturale, *Mem. Soc. Geol. Ital.*, *35*, 177–202.

- Patacca, E., P. Scandone, E. Di Luzio, G. P. Cavinato, and M. Parotto (2008), Structural architecture of the central Apennines: Interpretation of the CROP 11 seismic profile from the Adriatic coast to the orographic divide, *Tectonics*, *27*, TC3006, doi:10.1029/2005TC001917.
- Piana Agostinetti, N., and A. Amato (2009), Moho depth and v_p/v_s ratio in peninsular Italy from teleseismic receiver functions, *J. Geophys. Res.*, *114*, B06303, doi:10.1029/2008JB005899.
- Piana Agostinetti, N., and A. Malinverno (2010), Receiver function inversion by trans-dimensional Monte Carlo sampling, *Geophys. J. Int.*, *181*(2), 858–872, doi:10.1111/j.1365-246X.2010.04530.x.
- Sambridge, M. (1999), Geophysical inversion with a neighbourhood algorithm—I. Searching a parameter space, *Geophys. J. Int.*, *138*, 479–494.
- Savage, M. (1998), Lower crustal anisotropy or dipping boundaries? Effects on receiver functions and a case of study in New Zealand, *J. Geophys. Res.*, *103*(15), 69–87.
- Scisciani, V., and R. Montefalcone (2006), Coexistence of thin- and thick-skinned tectonics: An example for the central Apennines, Italy, *Spec. Pap. Geol. Soc. Am.*, *414*, 33–54.
- Scognamiglio, L., E. Tinti, A. Michelini, D. S. Dreger, A. Cirella, M. Cocco, S. Mazza, and A. Piatanesi (2010), Fast determination of moment tensors and rupture history: What has been learned from the 6 April 2009 L'Aquila earthquake sequence, *Seismol. Res. Lett.*, *81*, 892–906, doi:10.1785/gssrl.81.6.892.
- Sherrington, H. F., G. Zandt, and A. Frederiksen (2004), Crustal fabric in the Tibetan Plateau based on waveform inversion for seismic anisotropy parameters, *J. Geophys. Res.*, *109*, B02312, doi:10.1029/2002JB002345.
- Shiomi, K., and J. Park (2008), Structural features of the subducting slab beneath the Kii Peninsula, central Japan: Seismic evidence of slab segmentation, dehydration, and anisotropy, *J. Geophys. Res.*, *113*, B10318, doi:10.1029/2007JB005535.
- Walters, R. J., J. R. Elliott, N. D'Agostino, P. C. England, I. Hunstad, J. A. Jackson, B. Parsons, R. J. Phillips, and G. Roberts (2009), The 2009 L'Aquila earthquake (central Italy): A source mechanism and implications for seismic hazard, *Geophys. Res. Lett.*, *36*, L17312, doi:10.1029/2009GL039337.
- Wessel, P., and W. H. F. Smith (1991), Free software helps map and display data, *Eos Trans. AGU*, *72*(441), 445–446.

I. Bianchi, C. Chiarabba, and N. Piana Agostinetti, Istituto Nazionale di Geofisica e Vulcanologia, Centro Nazionale Terremoti, Via Vigna Murata 605, I-00143 Rome, Italy. (irene.bianchi@ingv.it)